Article

Experimental and Theoretical Study of the Reactions between Small Neutral Iron Oxide Clusters and Carbon Monoxide

Wei Xue, Zhe-Chen Wang, Sheng-Gui He, Yan Xie, and Elliot R. Bernstein

J. Am. Chem. Soc., **2008**, 130 (47), 15879-15888 • DOI: 10.1021/ja8023093 • Publication Date (Web): 31 October 2008

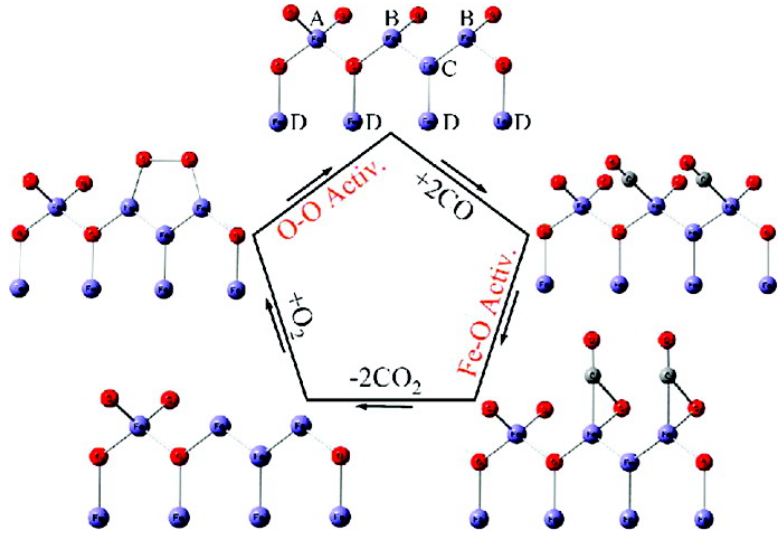

More About This Article

Additional resources and features associated with this article are available within the HTML version:

- Supporting Information
- Access to high resolution figures
- Links to articles and content related to this article
- Copyright permission to reproduce figures and/or text from this article

View the Full Text HTML

J|A|C|S
ARTICLES

Published on Web 10/31/2008

Experimental and Theoretical Study of the Reactions between Small Neutral Iron Oxide Clusters and Carbon Monoxide

Wei Xue,[†,‡] Zhe-Chen Wang,[†,‡] Sheng-Gui He,[*,†] Yan Xie,[§] and Elliot R. Bernstein[*,§]

Beijing National Laboratory for Molecular Sciences, State Key Laboratory for Structural Chemistry of Unstable and Stable Species, Institute of Chemistry, Chinese Academy of Sciences, Beijing 100080, People's Republic of China, Graduate School of the Chinese Academy of Sciences, Beijing 100080, People's Republic of China, and Department of Chemistry, Colorado State University, Fort Collins, Colorado 80523

Received March 30, 2008; E-mail: shengguihe@iccas.ac.cn; erb@lamar.colostate.edu

Abstract: Reactions of small *neutral* iron oxide clusters (FeO_{1-3} and $Fe_2O_{4,5}$) with carbon monoxide (CO) are investigated by experiments and first-principle calculations. The iron oxide clusters are generated by reaction of laser-ablation-generated iron plasma with O_2 in a supersonic expansion and are reacted with carbon monoxide in a fast flow reactor. Detection of the neutral clusters is through ionization with vacuum UV laser (118 nm) radiation and time-of-flight mass spectrometry. The FeO_2 and FeO_3 neutral clusters are reactive toward CO, whereas Fe_2O_4, Fe_2O_5, and possibly FeO are not reactive. A higher reactivity for FeO_2 [$\sigma(FeO_2 + CO) > 3 \times 10^{-17}$ cm^2] than for FeO_3 [$\sigma(FeO_3 + CO) \sim 1 \times 10^{-17}$ cm^2] is observed. Density functional theory (DFT) calculations are carried out to interpret the experimental observations and to generate the reaction mechanisms. The reaction pathways with negative or very small overall barriers are identified for CO oxidation by FeO_2 and FeO_3. The lower reactivity of FeO_3 with respect to FeO_2 may be related to a spin inversion process present in the reaction of FeO_3 with CO. Significant reaction barriers are calculated for the reactions of FeO and Fe_2O_{4-5} with CO. The DFT results are in good agreement with experimental observations. Molecular-level reaction mechanisms for CO oxidation by O_2, facilitated by condensed phase iron oxides as catalysts, are suggested.

1. Introduction

Transition metal oxides (TMOs) are an important group of industrial heterogeneous catalysts;[1] molecular-level mechanisms of many processes catalyzed by TMOs are, however, unclear. On the basis of the concept that a catalytic reaction occurs at specific catalytically active sites,[2] gas-phase metal oxide clusters composed of limited numbers of atoms that are fully accessible by both experiment and theory are excellent model systems with which to investigate the intrinsic reaction mechanisms for condensed phase catalytic processes.[3] On the other hand, discovery and understanding of TMO cluster chemistry may shed light on design, synthesis, and more effective use of TMO catalysts.

Kappes and Staley's landmark experimental investigation of CO oxidation by N_2O catalyzed by isolated FeO^+ (or Fe^+) in 1981 started the study of gas-phase molecular heterogeneous catalysis.[4] After more than 2 decades, many examples of catalytic cycles facilitated by metal atoms,[5] metal clusters,[6] and metal oxide clusters[7] have been demonstrated. Several excellent reviews are available in the literature.[8] Meanwhile, reactivity of TMO clusters toward various gas-phase molecules has been extensively investigated with emphasis on understanding the important step(s), such as bond activation, in practical catalytic

[†] Institute of Chemistry, Chinese Academy of Sciences.
[‡] Graduate School of the Chinese Academy of Sciences.
[§] Colorado State University.

(1) (a) Ertl, G.; Knozinger, H.; Weikamp, J. *Handbook of Heterogeneous Catalysis*; Wiley-VCH: Weinheim, Germany, 1997. (b) Horvath, I. T. *Encyclopedia of Catalysis*; Wiley International: New York, 2003. (c) Weckhuysen, B. M.; Keller, D. E. *Catal. Today* **2003**, *78*, 25. (d) Fierro, J. L. G. *Metal Oxides*; Taylor & Francis Group: Boca Raton, FL, 2006. (e) van Santen, R. A.; Neurock, M. *Molecular Heterogeneous Catalysis*; Wiley-VCH: Weinheim, Germany, 2006.
(2) (a) Zambelli, T.; Winterrin, J.; Frost, J.; Ertl, G. *Science* **1996**, *263*, 1688. (b) Bell, A. T. *Science* **2003**, *299*, 1688. (c) Thomas, J. M. *Top. Catal.* **2006**, *38*, 3.
(3) (a) Muetterties, E. L. *Science* **1977**, *196*, 839. (b) Jena, P.; Castleman, A. W., Jr. *Proc. Natl. Acad. Sci. U.S.A.* **2006**, *103*, 10560.
(4) Kappes, M. M.; Staley, R. H. *J. Am. Chem. Soc.* **1981**, *103*, 1286.
(5) (a) Baranov, V.; Javahery, G.; Hopkinson, A. C.; Böhme, D. K. *J. Am. Chem. Soc.* **1995**, *117*, 12801. (b) Brönstrup, M.; Schröder, D.; Kretzschmar, I.; Schwarz, H.; Harvey, J. N. *J. Am. Chem. Soc.* **2001**, *123*, 142. (c) Blagojevic, V.; Jarvis, M. J. Y.; Flaim, E.; Koyanagi, G. K.; Lavrov, V. V.; Böhme, D. K. *Angew. Chem.* **2003**, *115*, 5053; *Angew. Chem., Int. Ed.* **2003**, *42*, 4923. (d) Blagojevic, V.; Orlova, G.; Böhme, D. K. *J. Am. Chem. Soc.* **2005**, *127*, 3545.
(6) (a) Wallace, W. T.; Whetten, R. L. *J. Am. Chem. Soc.* **2002**, *124*, 7499. (b) Socaciu, L. D.; Hagen, J.; Bernhardt, T. M.; Wöste, L.; Heiz, U.; Häkkinen, H.; Landman, U. *J. Am. Chem. Soc.* **2003**, *125*, 10437. (c) Balaj, O. P.; Balteanu, I.; Rossteuscher, T. T. J.; Beyer, M. K.; Bondybey, V. E. *Angew. Chem.* **2004**, *116*, 6681; *Angew. Chem., Int. Ed.* **2004**, *47*, 6519.
(7) (a) Chiavarino, B.; Crestoni, M. E.; Fornarini, S. *Chem. Eur. J.* **2002**, *8*, 2740. (b) Waters, T.; O'Hair, R. A. J.; Wedd, A. G. *J. Am. Chem. Soc.* **2003**, *125*, 3384. (c) Wyrwas, R. B.; Jarrold, C. C. *J. Am. Chem. Soc.* **2006**, *128*, 13688.
(8) (a) O'Hair, R. A. J.; Khairallah, G. N. *J. Cluster Sci.* **2004**, *15*, 331. (b) Böhme, D. K.; Schwarz, H. *Angew. Chem., Int. Ed.* **2005**, *44*, 2336. (c) Schröder, D.; Schwarz, H. *Top. Organomet. Chem.* **2007**, *22*, 1.

cycles.[9] Since mass spectrometric techniques are widely used for this research, most studies of TMO cluster reactivity are for ionic TMO clusters. Reactivity of neutral TMO clusters has not been studied experimentally, to the best of our knowledge. Considerable experimental effort, however, has been expended to study the reactivity of neutral diatomic TMOs and some neutral polyatomic species by spectroscopic methods; for example, laser-induced fluorescence (LIF) or infrared (IR) absorption studies have been reported for neutral species.[10,11] The importance of studying the reactivity of *neutral*, in addition to ionic, clusters can be seen from a theoretical investigation of methanol oxidation to formaldehyde on supported vanadium oxide catalysts.[12] The investigation concludes that the neutral $O{=}V(OCH_3)_3$ molecule is a suitable gas-phase model for studying the rate-limiting step (transfer of a methyl H atom to vanadyl O atom), whereas the $O{=}V(OCH_3)_3^+$ cationic radical is not.

The reason that only ionic TMO clusters are studied by mass spectrometry is that electric and magnetic forces can be used to control and manipulate charged species; in contrast, neutral clusters are difficult to control and usually must be ionized for detection. The ionization of a neutral TMO cluster by typical methods such as electron impact or multiphoton ionization techniques almost always causes cluster fragmentation. The TMO cluster fragmentation during ionization prevents parent molecule identification because the different neutral clusters created are usually mixed together and their fragmentation patterns interfere with reactivity studies. Single-photon ionization (SPI) with vacuum ultraviolet (VUV) and soft X-ray lasers has been recently demonstrated to be a successful technique for detecting neutral TMO clusters without fragmentation.[11,13] SPI is used in this study to investigate reactivity of neutral iron oxide clusters (Fe_mO_n) toward CO. This technique has recently been applied to study reactivity of neutral vanadium oxide clusters toward C_2 hydrocarbons.[14]

Low-temperature, low-cost, and efficient CO oxidation (removal) can solve serious environmental problems that are caused by CO emission from automobiles, industrial processing, and even cigarette burning. The CO oxidation is also important in other areas such as respiratory protection and fuel gas cleanup. Iron oxides (Fe_xO_y) have been extensively studied as noble metal free catalysts for low-temperature CO oxidation.[15−19] In early studies,[15] the prepared iron oxide catalysts are only active for CO oxidation at high temperatures (>673 K). Li et al.[16] found that nanosized iron oxide can be highly catalytic at much lower temperature (523 K), which is confirmed in various other independent studies.[17] Specially prepared and treated nanosized iron oxides are found to be catalytic even at ambient conditions ($T \approx 300$ K).[18,19] Measured apparent activation energies for the oxidation of CO by O_2 are higher for non-nano Fe_2O_3 powder (~83.7 kJ/mol[15a]) than for Fe_2O_3 nanoparticles (60.7 kJ/mol,[16] 26.4 kJ/mol[17b]). CO can be readily oxidized by Fe_2O_3 nanoparticles in the absence of O_2.[16,17b]

These investigations, as well as others, employing alternative oxides (Mn_xO_y, Co_xO_y, Ni_xO_y,...)[20] are important to find efficient noble metal free catalysts for the oxidation of CO; however, from these studies, the intrinsic reaction mechanism, or how CO oxidation gets catalyzed at a molecular level, is still not clear. Various mechanism issues arise in these condensed phase investigations. Li et al. concluded that the small particle size and the FeOOH component of their Fe_2O_3 catalyst contribute to the high catalytic performance.[16] Zheng et al. concluded that the high density of Fe atoms on the exposed {110} planes of their quasicubic α-Fe_2O_3 nanoparticles leads to the excellent catalytic reactivity.[17d] Szegedi et al. concluded that both ionic and metallic forms of iron are active in low-temperature CO oxidation.[18] Gas-phase investigations of reactions of various Fe_mO_n clusters with CO will provide a good model for the understanding of the intrinsic mechanisms of CO interaction with active sites of condensed phase catalysts.

Gas-phase reactions of ionic iron oxide clusters ($Fe_{1-2}O_n^+$, $Fe_{1-2}O_n^-$) with low-pressure (less than 20 mTorr) CO gas have been recently investigated.[21] First-principle calculations have also been applied to interpret the experimental results. The Fe−O bond strength of cationic clusters is usually weaker than that of anionic species.[22] As a result, FeO_n^+ ($n = 1-3$) are more reactive than FeO_n^- toward CO oxidation.[21a] First-principle calculations were also used by Reddy and co-workers to study CO oxidation catalyzed by a neutral Fe_2O_3 cluster.[23] CO adsorption onto gas-phase Fe_2O_3 clusters causes rearrangement of one of the three Fe−O−Fe bridged bonds to one Fe−O terminal bond. A reaction barrier of 0.39 eV is calculated for

(9) (a) Fialko, E. F.; Kikhtenko, A. V.; Goncharov, V. B.; Zamaraev, K. I. *J. Phys. Chem. A* **1997**, *101*, 8607. (b) Armentrout, P. B. *Annu. Rev. Phys. Chem.* **2001**, *52*, 423. (c) Zemski, K. A.; Justes, D. R.; Castleman, A. W., Jr. *J. Phys. Chem. B* **2002**, *106*, 6136, and references therein. (d) Justes, D. R.; Mitric, R.; Moore, N. A.; Bonacic-Koutecký, V.; Castleman, A. W., Jr. *J. Am. Chem. Soc.* **2003**, *125*, 6289. (e) Justes, D. R.; Moore, N. A.; Castleman, A. W., Jr. *J. Phys. Chem. B* **2004**, *108*, 3855. (f) Kimble, M. L.; Castleman, A. W., Jr.; Mitric, R.; Bürgel, C.; Bonacic-Koutecky, V. *J. Am. Chem. Soc.* **2004**, *126*, 2526. (g) Feyel, S.; Schröder, D.; Rozanska, X.; Sauer, J.; Schwarz, H. *Angew. Chem., Int. Ed.* **2006**, *45*, 4677. (h) Feyel, S.; Dobler, J.; Schröder, D.; Sauer, J.; Schwarz, H. *Angew. Chem., Int. Ed.* **2006**, *45*, 4681. (i) Operti, L.; Rabezzana, R. *Mass Spectrom. Rev.* **2006**, *25*, 483, and references therein.

(10) (a) Plane, J. M. C.; Rollason, R. J. *Phys. Chem. Chem. Phys.* **1999**, *1*, 1843. (b) Rollason, R. J.; Plane, J. M. C. *Phys. Chem. Chem. Phys.* **2000**, *2*, 2335. (c) Wang, G.; Gong, Y.; Chen, M.; Zhou, M. *J. Am. Chem. Soc.* **2006**, *128*, 5974.

(11) Matsuda, Y.; Bernstein, E. R. *J. Phys. Chem. A* **2005**, *109*, 3803.

(12) Döbler, J.; Pritzsche, M.; Sauer, J. *J. Am. Chem. Soc.* **2005**, *127*, 10861.

(13) (a) Matsuda, Y.; Bernstein, E. R. *J. Phys. Chem. A* **2005**, *109*, 314. (b) Matsuda, Y.; Shin, D. N.; Bernstein, E. R. *J. Chem. Phys.* **2004**, *120*, 4142. (c) Shin, D. N.; Matsuda, Y.; Bernstein, E. R. *J. Chem. Phys.* **2004**, *120*, 4157. (d) Matsuda, Y.; Shin, D. N.; Bernstein, E. R. *J. Chem. Phys.* **2004**, *120*, 4165. (e) Dong, F.; Heinbuch, S.; He, S.-G.; Xie, Y.; Rocca, J. J.; Bernstein, E. R. *J. Chem. Phys.* **2006**, *125*, 164318.

(14) Dong, F.; Heinbuch, S.; Xie, Y.; Rocca, J. J.; Bernstein, E. R.; Wang, Z.-C.; Deng, K.; He, S.-G. *J. Am. Chem. Soc.* **2008**, *130*, 1932.

(15) (a) Walker, J. S.; Straguzzi, G. I.; Manogue, W. H.; Schuit, G. C. A. *J. Catal.* **1988**, *110*, 299. (b) Uddin, M. A.; Komatsu, T.; Yashima, T. *J. Catal.* **1994**, *146*, 468.

(16) Li, P.; Miser, D. E.; Rabiei, S.; Yadav, R. T.; Hajaligol, M. R. *Appl. Catal., B* **2003**, *43*, 151.

(17) (a) Xiong, Y.; Li, Z.; Li, X.; Hu, B.; Xie, Y. *Inorg. Chem.* **2004**, *43*, 6540. (b) Khedr, M. H.; Abdel Halim, K. S.; Nasr, M. I.; El-Mansy, A. M. *Mater. Sci. Eng., A* **2006**, *430*, 40. (c) Hu, C.; Gao, Z.; Yang, X. *Chem. Lett.* **2006**, *35*, 1288. (d) Zheng, Y.; Cheng, Y.; Wang, Y.; Bao, F.; Zhou, L.; Wei, X.; Zhang, Y.; Zheng, Q. *J. Phys. Chem. B* **2006**, *110*, 3093.

(18) Szegedi, Á.; Hegedüs, M.; Margitfalvi, J. L.; Kiricsi, I. *Chem. Commun.* **2005**, 1441.

(19) Lin, H.; Chen, Y.; Wang, W. *J. Nanopart. Res.* **2005**, *7*, 249.

(20) (a) Jansson, J.; Palmqvist, A. E. C.; Fridell, E.; Skoglundh, M.; Qsterlund, L.; ThormRhlen, P.; Langer, V. *J. Catal.* **2002**, *211*, 387. (b) Saalfrank, J. W.; Maier, W. F. *Angew. Chem., Int. Ed.* **2004**, *43*, 2028.

(21) (a) Reilly, N. M.; Reveles, J. U.; Johnson, G. E.; Khanna, S. N.; Castleman, A. W., Jr. *Chem. Phys. Lett.* **2007**, *435*, 295. (b) Reilly, N. M.; Reveles, J. U.; Johnson, G. E.; Khanna, S. N.; Castleman, A. W., Jr. *J. Phys. Chem. A* **2007**, *111*, 4158. (c) Reilly, N. M.; Reveles, J. U.; Johnson, G. E.; del Campo, J. M.; Khanna, S. N.; Castleman, A. W., Jr. *J. Phys. Chem. C* **2007**, *111*, 19086.

CO approaching the Fe_2O_3 cluster. The Fe−O terminal bond can further oxidize another CO molecule to form CO_2 easily. There is, unfortunately, no gas-phase experimental study to support the calculated results for the neutral cluster.

Properties of gas-phase iron oxide clusters are extensively studied by LIF,[10a,b,24] IR,[25] photoelectron spectroscopy,[26] mass spectrometry,[13c,27] as well as quantum chemistry calculations.[5d,10a,b,25,26c,28] Generally, the theoretical results are reliable enough to help in the interpretation of experimental data. For a few cases, analysis of the theoretical results has to be guided by experimental data. One example of this latter case is the determination of the ground state of the FeO_2 molecule. The experimental data suggest that FeO_2 possesses a triplet ground state, but some often-used theoretical methods predict a quintet ground state.[25] In this study, density functional theory (DFT) calculations and SPI techniques are used to investigate the reactivity of neutral Fe_mO_n clusters toward CO. The experimental results are well interpreted by the calculations. Details of the reaction mechanism are obtained and used to interpret the condensed phase catalytic process of CO oxidation by O_2 over iron oxides at a molecular level.

2. Methods

2.1. Experimental Methods. The experimental setup for a pulsed laser-ablation/supersonic nozzle coupled with a fast flow reactor has been described in previous studies.[14,29] Only a brief outline of the experiments is given below. Fe_mO_n clusters are generated by laser ablation of iron metal foil in the presence of 10% O_2 seeded in a He carrier gas with typical backing pressure of 75 psi. A 532 nm (second harmonic of Nd^{3+}:yttrium aluminum garnet−YAG) laser with energy of 5−8 mJ/pulse and repetition rate of 10 Hz is used. The gas is controlled by a pulsed nozzle made by the R. M. Jordan Company. The clusters formed in a gas channel (2 mm diameter × 19 mm length) are expanded and reacted with CO or other gas molecules (O_2, NO,...) seeded in He in a fast flow reactor (6 mm diameter × 76 mm length). The reactant gases (CO seeded in He) with typical backing pressure of 10 psi are pulsed into the reactor 20 mm downstream from the exit of the narrow cluster formation channel by a second pulsed valve (General Valve, series 9). The instantaneous gas pressure in the fast flow reactor is estimated (see references and notes in ref 30) to be around 14 Torr during the time that the second nozzle is opening. Oxide clusters exiting the narrow cluster formation channel are usually rotationally cold ($T_{rot} \sim 50$ K) and vibrationally hot ($T_{vib} \sim 700$ K).[11] The number of collisions that a cluster (radius = 0.25 nm) experiences with the bath gas (radius = 0.05 nm, $T = 350$ K, $P = 14$ Torr) in the fast flow reactor is about 100 per 1 mm of forward motion. This corresponds to a collision rate of 10^8 s^{-1} for an approaching velocity of 1 km/s. Considering that the reactor length (76 mm) is much longer than 1 mm, the intracluster vibrations are likely equilibrated to the bath gas temperature before reacting with the diluted (1−5%) reactant gas. The bath gas temperature is around 300−400 K considering that the carrier gas can be heated during the process of laser ablation (see ref 30b for details).

After reacting in the fast flow reactor, ions are deflected from the molecular beam by an electric field located 5 mm downstream from the fast flow reactor. The neutral reactants and products exiting from the reactor are skimmed (5 mm diameter) into a vacuum system of a time-of-flight mass spectrometer (TOFMS) for ionization by a VUV laser with output at 118 nm, 10.5 eV. Ions are detected and signals are recorded as previously described.[13c,27a] The uncertainty of the reported relative mass signals in this study is about 10%. The 118 nm laser light is generated by focusing the third harmonic (355 nm, ~30 mJ/pulse) of a Nd:YAG laser in a tripling cell that contains about a 250 Torr argon/xenon (10/1) gas mixture. To separate the generated 118 nm laser beam from the 355 nm fundamental beam, a magnesium fluoride prism (made by Crystaltechno Ltd., Russia, apex angle = 6°), which was not employed in our previous studies,[11,13a−d] is inserted into the light path. In this case, one is quite certain that the mass signals are generated by ionization purely through the VUV laser radiation with low power (~1 μJ/pulse, pulse duration ~5 ns).

2.2. Computational Methods. The DFT calculations using the Gaussian 03 program[31] have been employed to study the reactions of neutral Fe_mO_n clusters with CO and O_2. The reaction pathways are followed for $FeO_{1-3} + CO \rightarrow FeO_{0-2} + CO_2$, $Fe_2O_{3-5} + CO \rightarrow Fe_2O_{2-4} + CO_2$, $FeO + O_2 \rightarrow FeO_3$, and $Fe_2O_{1-3} + O_2 \rightarrow Fe_2O_{3-5}$. The reaction pathway calculations involve geometry

(22) (a) Metz, R. B.; Nicolas, C.; Ahmed, M.; Leone, S. R. *J. Chem. Phys.* **2005**, *123*, 114313. (b) Chestakov, D. A.; Parker, D. H.; Baklanov, A. V. *J. Chem. Phys.* **2005**, *122*, 084302. (c) Valli, C.; Blondel, C.; Delsart, C. *Phys. Rev. A* **1999**, *59*, 3809. (d) Leopold, D. G.; Lineberger, W. C. *J. Chem. Phys.* **1986**, *85*, 51. (e) Drechsler, G.; Boesl, U.; Bäβmann, C.; Schlag, E. W. *J. Chem. Phys.* **1997**, *107*, 2284 (f) Notes: The experimental bond strength (D_0) for FeO^+ is $D_0(Fe^+-O) = 3.52 \pm 0.02$ eV (ref 22a). The experimental D_0 values for FeO^- are $D_0(Fe^--O) = D_0(Fe-O) + EA(FeO)-EA(Fe) = 5.52 \pm 0.01$ eV and $D_0(Fe-O^-) = D_0(Fe-O) + EA(FeO)-EA(O) = 4.21 \pm 0.01$ eV, in which $D_0(Fe-O) = 4.18 \pm 0.01$ eV (ref 22b) and EA denotes electron affinity: $EA(O) = 1.46111 \pm 0.00004$ eV (ref 22c), $EA(Fe) = 0.151 \pm 0.003$, (ref 22d), and $EA(FeO) = 1.4945 \pm 0.0002$ eV (ref 22e). The calculated D_0 values for FeO_n^+ ($n = 1-3$) are all less than 4.75 eV, whereas those for FeO_n^- ($n = 1-3$) are all greater than 5.75 eV in ref 21a.

(23) (a) Reddy, B. V.; Rasouli, F.; Hajaligol, M. R.; Khanna, S. N. *Chem. Phys. Lett.* **2004**, *384*, 242. (b) Reddy, B. V.; Rasouli, F.; Hajaligol, M. R.; Khanna, S. N. *Fuel* **2004**, *83*, 1537. (c) Reddy, B. V.; Khanna, S. N. *Phys. Rev. Lett.* **2004**, *93*, 068301.

(24) Steimle, T. C.; Nachman, D. F.; Shirley, J. E.; Merer, A. J. *J. Chem. Phys.* **1989**, *90*, 5360.

(25) (a) Andrews, L.; Chertihin, G. V.; Ricca, A.; Bauschlicher, C. W., Jr. *J. Am. Chem. Soc.* **1996**, *118*, 467. (b) Chertihin, G. V.; Saffel, W.; Yustein, J. T.; Andrews, L.; Neurock, M.; Ricca, A.; Bauschlicher, C. W., Jr. *J. Phys. Chem.* **1996**, *100*, 5261.

(26) (a) Wu, H.; Desai, S. R.; Wang, L. S. *J. Am. Chem. Soc.* **1996**, *118*, 5296. (b) Wang, L. S.; Wu, H.; Desai, S. R. *Phys. Rev. Lett.* **1996**, *76*, 4853. (c) Gutsev, G. L.; Bauschlicher, C. W., Jr.; Zhai, H. J.; Wang, L. S. *J. Chem. Phys.* **2003**, *119*, 11135.

(27) (a) Shin, D. N.; Matsuda, Y.; Bernstein, E. R. *J. Chem. Phys.* **2004**, *120*, 4150. (b) Schröder, D.; Fiedler, A.; Schwarz, J.; Schwarz, H. *Inorg. Chem.* **1994**, *33*, 5094. (c) Schröder, D.; Roithova, J.; Schwarz, H. *Int. J. Mass Spectrom.* **2006**, *254*, 197. (d) Molek, K. S.; Anfuso-Cleary, C.; Duncan, M. A. *J. Phys. Chem. A* **2008**, *112*, 9238.

(28) (a) Cao, Z.; Duran, M.; Sola, M. *Chem. Phys. Lett.* **1997**, *274*, 411. (b) Gutsev, G. L.; Khanna, S. N.; Rao, B. K.; Jena, P. *J. Phys. Chem. A* **1999**, *103*, 5812. (c) Kellogg, C. B.; Irikura, K. K. *J. Phys. Chem. A* **1999**, *103*, 1150. (d) García-Sosa, A. T.; Castro, M. *Int. J. Quantum Chem.* **2000**, *80*, 307. (e) Shiroishi, H.; Oda, T.; Hamada, I.; Fujima, N. *Polyhedron* **2005**, *24*, 2472.

(29) Xie, Y.; He, S.-G.; Dong, F.; Bernstein, E. R. *J. Chem. Phys.* **2008**, *128*, 044306.

(30) (a) Anderson, J. B. In *Molecular Beams and Low Density Gas Dynamics*; Wegner, P. P., Ed.; Marcel Dekker: New York, 1974. (b) Geusic, M. E.; Morse, M. D.; O'Brien, S. C.; Smalley, R. E. *Rev. Sci. Instrum.* **1985**, *56*, 2123 (c) Notes: The pressure (P) is calculated with the ideal gas law $P = nkT$ in which k and T are the Boltzmann constant and the gas temperature, respectively. The molecular density (n) is determined by $n = F/A/C$ (refs 30a and b) in which F is the gas flow rate (in molecule/s), A is the cross-sectional area defined by the inner diameter of the fast flow reactor, and C [$= (\gamma kT/m)^{1/2}$; parameters of helium are used: $\gamma = 5/3$ and m = mass of He atom] is the speed of sound. The gas flow rate F is determined as $F = N/\Delta$ where N is number of gas molecules per pulse injected from the second nozzle and Δ is the duration of gas pulse (2.0 ms in our experiment). The (average) N value is quite accurately determined by monitoring the amount of gas (~5% uncertainty) injected into the vacuum after running the pulsed valve (at 10 Hz) for a fixed period of time. The uncertainty of n originates mainly from the indirect determination of Δ that is read directly from the pulse duration of the voltage that drives the solenoid valve. The uncertainty of Δ is about 30%. $n_{CO} = (3.85 \pm 1.16) \times 10^{15}$ and $(1.92 \pm 0.58) \times 10^{16}$ cm^{-3} are determined for 1% and 5% CO conditions, respectively.

(31) Frisch, M. J.; et al. Gaussian 03 , revision C.02; Gaussian, Inc.: Wallingford, CT, 2004.

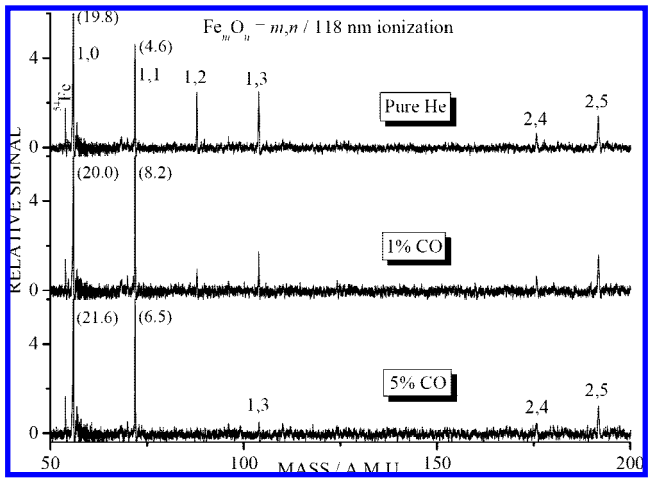

Figure 1. TOF mass spectra for reaction of neutral iron oxide clusters with carbon monoxide in a fast flow reactor. The CO concentrations are 0% (top trace), 1% (middle), and 5% (bottom) in the helium carrier gas. The relative signals of Fe and FeO are given in the parentheses.

optimizations of various reaction intermediates and transition states through which the intermediates transfer to each other. The transition state optimizations are performed by employing either the Berny algorithm[32] or the synchronous transit-guided quasi-Newton (STQN) method.[33] Vibrational frequency calculations are performed to check that reaction intermediates and transition state species have zero and one imaginary frequencies, respectively. Intrinsic reaction coordinate (IRC) calculations[34] are also performed so that a transition state connects two appropriate local minima in the reaction pathways. The hybrid B3LYP exchange-correlation functional[35] is used. The basis set adopted is the triply split 6-311+G* basis set[36] with one set of diffuse and polarization functions[37] for all atoms. The same methods were successfully used to study the reaction mechanisms of $N_2O + CO \rightarrow N_2 + CO_2$ catalyzed by Fe^+ (or FeO^+).[5d] Relative free energies under standard conditions (298.15 K, 1 atm) are reported. Cartesian coordinates, energies, and vibrational frequencies for all of the optimized structures are listed as tables in the Supporting Information.

3. Results

3.1. Experimental Results. Figure 1 presents TOF mass spectra for the reactions of neutral Fe_mO_n clusters with 0% (reference), 1%, and 5% CO seeded in He in the fast flow reactor. The mass signal of FeO_2 disappears completely after it reacts with 5% CO at ca. 300−400 K, whereas no apparent signal depletion is observed for Fe_2O_4 and Fe_2O_5 under the same conditions. Significant signal depletion of FeO_3 is observed after the reaction with CO. The reaction cross section (σ) or first-order rate constant (k_1) in the fast flow reactor can be estimated by using the following equation:

$$I_{gas} = I_{He} \exp(-\sigma n l) = I_{He} \exp(-k_1 n \Delta t) \quad (1)$$

in which I_{gas} and I_{He} are signal magnitudes of the clusters after reaction/collision with reactant gas (CO) and pure He, respectively, n is the molecular density of reactant gas (the estimation of n is given as notes in ref 30c), l is the effective path length of the reactor (~76 mm), and Δt is the reaction time that can be estimated as $\Delta t = l/v$ (v—the cluster beam velocity ~1 km/s). To obtain the uncertainties of σ and k_1 in eq 1, uncertainties of 30% are given for n,[30c] 20% for l, and 10% for the rest of the independent quantities (I_{gas}, I_{He}, and v).

Using the relative signal magnitudes of FeO_3 from the middle ($I_{1\%\ CO}/I_{He} = 1.75/2.58$) and bottom ($I_{5\%\ CO}/I_{He} = 0.61/2.58$) spectra in Figure 1, the reaction cross sections $\sigma(FeO_3 + CO) = (1.3 \pm 0.7) \times 10^{-17}$ and $(1.0 \pm 0.4) \times 10^{-17}$ cm^2 are determined, respectively. The corresponding rate constant is $k_1(FeO_3 + CO) = (1.3 \pm 0.7) \times 10^{-12}$ and $(1.0 \pm 0.4) \times 10^{-12}$ cm^3 molecule^{-1} s^{-1}. The difference of $\sigma(FeO_3 + CO)$ determined at different concentrations of CO is within the experimental uncertainties. Similar calculation can be applied to $FeO_2 + CO$ using the relative signal magnitudes of FeO_2 ($I_{1\%\ CO}/I_{He} = 0.92/2.46$). This leads to $\sigma(FeO_2 + CO) = (3.4 \pm 1.3) \times 10^{-17}$ cm^2. The calculation of $\sigma(FeO_2 + CO)$ using eq 1 does not take into account the complication that some FeO_2 may be formed from the reaction of $FeO_3 + CO \rightarrow FeO_2 + CO_2$. As a result, the above calculation gives the lower limit for $\sigma(FeO_2 + CO)$. Considering a consecutive first-order reaction involving two stages[38] ($FeO_3 + CO \rightarrow FeO_2 + CO_2$, $FeO_2 + CO \rightarrow FeO + CO_2$) and assuming the ionization efficiencies of FeO_2 and FeO_3 are the same, the corrected[38c] reaction cross section $\sigma^{corr}(FeO_2 + CO) = (5.3 \pm 2.1) \times 10^{-17}$ cm^2 is obtained.

The reactions of charged FeO_2^- and FeO_2^+ with CO have been studied under well-defined conditions,[21b,c] for which a cluster signal decrease of 9%/25% is observed for FeO_2^-/FeO_2^+ reacting with 20/5 mTorr CO in a gas cell with an effective path length of 12.9 cm.[39] By using eq 1 and $T = 305$ K,[39] $\sigma(FeO_2^- + CO) = 1.2 \times 10^{-17}$ cm^2 and $\sigma(FeO_2^+ + CO) = 14.2 \times 10^{-17}$ cm^2 are obtained. Interestingly, the $\sigma^{corr}(FeO_2 + CO)$ determined in this work is in between $\sigma(FeO_2^+ + CO)$ and $\sigma(FeO_2^- + CO)$.

In Figure 1, the signal of FeO first increases, then decreases, as the CO concentration increases. This can be interpreted by relatively quick reactions of $FeO_2 + CO \rightarrow FeO + CO_2$ and $FeO_3 + 2CO \rightarrow FeO + 2CO_2$ and slow reaction of $FeO + CO \rightarrow Fe + CO_2$. Because the relative ionization efficiencies of FeO, FeO_2, and FeO_3 are unknown, the estimation of $\sigma(FeO + CO)$ is not given in this study. Under the 5% CO condition, the FeO_2 signal disappears completely, whereas the FeO signal is still higher than that under pure He conditions. We conclude that FeO_2 is more reactive than FeO and that it is the most reactive cluster among FeO_{1-3} and Fe_2O_{4-5} in the reaction with CO.

Reactions of Fe_mO_n clusters with other gases are also studied to test the reaction selectivity of Fe_mO_n. The results are shown

(32) Schlegel, H. B. *J. Comput. Chem.* **1982**, *3*, 214.
(33) (a) Peng, C.; Schlegel, H. B. *Isr. J. Chem.* **1994**, *33*, 449. (b) Peng, C.; Ayala, P. Y.; Schlegel, H. B.; Frisch, M. J. *J. Comput. Chem.* **1996**, *17*, 49.
(34) (a) Gonzalez, C.; Schlegel, H. B. *J. Chem. Phys.* **1989**, *90*, 2154. (b) Gonzalez, C.; Schlegel, H. B. *J. Phys. Chem.* **1990**, *94*, 5523.
(35) (a) Becke, A. D. *Phys. Rev. A* **1988**, *98*, 3098. (b) Becke, A. D. *J. Chem. Phys.* **1993**, *98*, 5648. (c) Lee, C.; Yang, W.; Parr, R. G. *Phys. Rev. B* **1998**, *37*, 785.
(36) (a) Hehre, W. J.; Ditchfield, R.; Pople, J. A. *J. Chem. Phys.* **1972**, *56*, 2257. (b) Krishnan, R.; Binkley, J. S.; Seeger, R.; Pople, J. A. *J. Chem. Phys.* **1980**, *72*, 650.
(37) (a) Chandrasekhar, J.; Andrade, J. G.; Schleyer, P. v. R. *J. Am. Chem. Soc.* **1981**, *103*, 5609. (b) Clark, T.; Chandrasekhar, J.; Spitznagel, G. W.; Schleyer, P.v. R. *J. Comput. Chem.* **1983**, *4*, 294.
(38) Steinfeld, J. I.; Francisco, J. S.; Hase, W. L. *Chemical Kinetics and Dynamics*; Prentice-Hall: Upper Saddle River, NJ, 1999; (a) p 26 and (b) pp 313−314. (c) Determination of $\sigma^{corr}(FeO_2 + CO)$ involves finding solution for x in a nonlinear equation: $Ae^{-x} + B(1-e^{-x})/x - C = 0$, in which $A = I_{He}(FeO_2)/I_{He}(FeO_3)$, $B = -\ln[I_{gas}(FeO_3)/I_{He}(FeO_3)]$, $C = I_{gas}(FeO_2)/I_{gas}(FeO_3)$, and $\sigma^{corr}(FeO_2 + CO) = (x + B)/nl$. The uncertainty of $x + B$ is determined by calculations of the numerical derivatives of $x + B$ with respect to the independent mass signal magnitudes (I_{gas} and I_{He} with 10% uncertainty).
(39) Bell, R. C.; Zemski, K. A.; Justes, D. R.; Castleman, A. W., Jr. *J. Chem. Phys.* **2001**, *114*, 798.

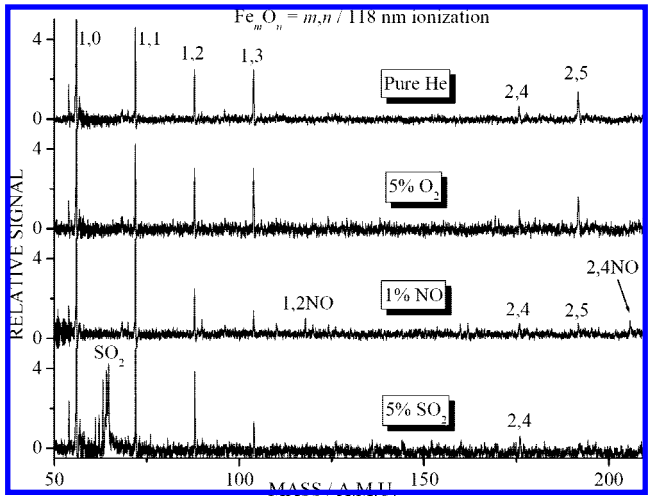

Figure 2. TOF mass spectra for reaction of neutral iron oxide clusters with 5% O_2, 1% NO, and 5% SO_2. 1,2NO and 2,4NO denote product peaks of FeO_2NO and Fe_2O_4NO, respectively.

in Figure 2 for O_2, NO, and SO_2 as reactant gases. No reaction between Fe_mO_n and O_2 is observed. The reactivity of neutral Fe_mO_n toward NO and SO_2 is quite different from that toward CO: Fe_2O_5 reacts with NO and SO_2, whereas FeO_2 is less or nonreactive with these two gases. FeO_3 is also reactive with NO and SO_2. Two products, FeO_2NO and Fe_2O_4NO (possibly from association reactions X + NO → XNO, in which X = FeO_2 and Fe_2O_4), are observed for NO as the reactant gas. On the basis of the experimental (for NO_2 and SO_3)[40] and calculated (for FeO_3 and Fe_2O_5, see section 4.1) bond enthalpies of related species, NO and SO_2 may be oxidized by FeO_3 and Fe_2O_5, i.e., $FeO_3 + NO/SO_2 \rightarrow FeO_2 + NO_2/SO_3$, $Fe_2O_5 + NO/SO_2 \rightarrow Fe_2O_4 + NO_2/SO_3$.

The size-dependent reactivity of iron oxide clusters toward CO (see Figure 1) is interesting. In this study, reaction mechanisms of FeO_{1-3} and Fe_2O_{4-5} with CO are interpreted based on quantum chemistry calculations.

3.2. Computational Results. To gauge the validity of the B3LYP/6-311+G* method for calculation of reaction pathways for CO oxidation by Fe_mO_n and Fe_mO_n oxidation by O_2, bond enthalpies (H_b), as well as bond lengths, are calculated and compared with experimental values[22b,40,41] for O_2, CO, CO_2, and FeO molecules. The comparison is made in Table S1 (see the Supporting Information). The B3LYP functional shows excellent performance for bond length (within 0.002 Å) calculations. This functional underestimates H_b of CO by 0.32 eV. The H_b values of O_2, CO_2, and FeO are well (within 0.07 eV) calculated through the B3LYP functional. We expect that the relative energetics for $Fe_mO_n + CO \rightarrow Fe_mO_{n-1} + CO_2$ and $Fe_mO_n + O_2 \rightarrow Fe_mO_{n+2}$ can be reasonably predicted by B3LYP/6-311+G*, as long as the calculated H_b values of Fe_mO_n are accurate enough. The BPW91 functional, which has a good performance for electron affinity calculations,[28b] overestimates H_b values, and the largest error (~1 eV) occurs for FeO. B3PW91 shows a similar performance to B3LYP for main group species O_2, CO, and CO_2, whereas the bond length and the H_b value of FeO are not very well calculated. All the reaction pathways reported in this study are calculated at the B3LYP/6-311+G* level. In general, the choice between B3LYP and BPW91 seems to depend upon just what properties and systems one wishes to emphasize.

Figures 3−5 plot the DFT calculated reaction pathways for CO oxidation by FeO, FeO_2, and FeO_3, respectively. FeO has a quintet ground state ($^5\Delta$). A significant overall reaction barrier

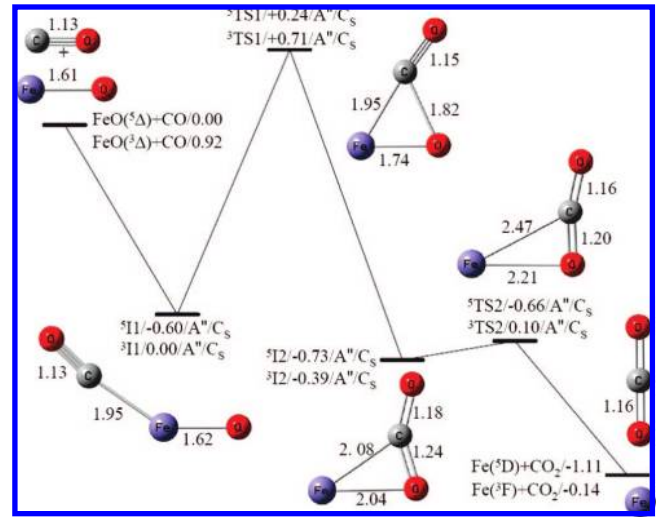

Figure 3. DFT calculated reaction pathways for FeO ($^5\Delta$) + CO ($^1\Sigma^+$) → Fe (^{5}D) + CO_2 ($^1\Sigma_g^+$) and FeO ($^3\Delta$) + CO ($^1\Sigma^+$) → Fe (^{3}F) + CO_2 ($^1\Sigma_g^+$). The reaction intermediates and transition states are denoted as ^{M}I*n* and ^{M}TS*n*, respectively, where the superscript *M* indicates the spin multiplicities. The relative Gibbs free energy at 298 K (ΔG_{298K} in eV), electronic configuration (Γ), and the point group (PG) of the species are given as $\Delta G_{298K}/\Gamma$/PG. The bond lengths in 0.1 nm are given. All of the energies are relative to the total free energy of FeO ($^5\Delta$) and CO ($^1\Sigma^+$). The energy profile and structures in this figure are plotted for the FeO ($^5\Delta$) + CO ($^1\Sigma^+$) reaction.

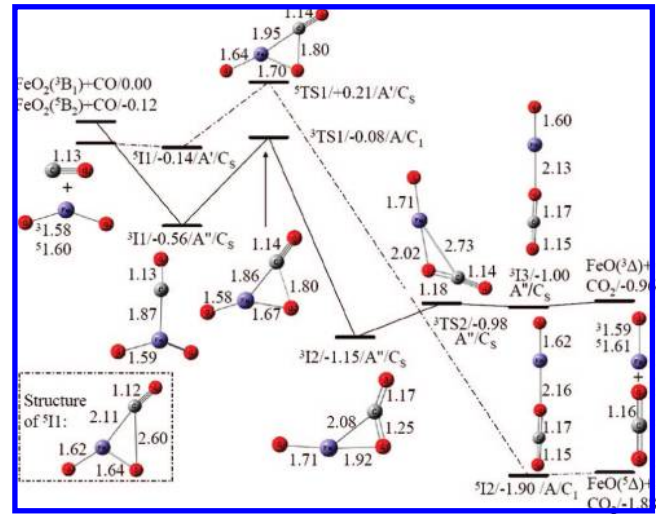

Figure 4. DFT calculated reaction pathways for FeO_2 ($^3B_1$) + CO ($^1\Sigma^+$) → FeO ($^3\Delta$) + CO_2 ($^1\Sigma_g^+$) and FeO_2 ($^5B_2$) + CO ($^1\Sigma^+$) → FeO ($^5\Delta$) + CO_2 ($^1\Sigma_g^+$). See the caption of Figure 3 for explanations. All of the energies are relative to the total free energy of FeO_2 ($^3B_1$) and CO ($^1\Sigma^+$).

Figures 3−5 plot the DFT calculated reaction pathways for CO oxidation by FeO, FeO_2, and FeO_3, respectively. FeO has a quintet ground state ($^5\Delta$). A significant overall reaction barrier

(40) Chase, M. W. NIST−JANAF Themochemical Tables, 4th ed. *J. Phys. Chem. Ref. Data* Monograph 9, **1998**.

(41) (a) Wells, A. F. *Structural Inorganic Chemistry*, 4th ed. Clarendon Press: Oxford, 1975. (b) Cheung, A. S. C.; Lee, N.; Lyyra, A. M.; Merer, A. J.; Taylor, A. W. *J. Mol. Spectrosc.* **1982**, *95*, 213.

(42) The adopted B3LYP/6-311+G* method predicts that the quintet $FeOO_2$ (FeO_3 molecule containing −O−O− moiety, $^5B_2$, C_{2v} symmetry, see ^{5}I2 in Supporting Information Figure S7) is only above the ground-state FeO_3 ($^1A_1'$, D_{3h}) by 0.032 eV (zero-point-vibration corrected, see Tables S4 and S11 in the Supporting Information). Considering that the B3LYP functional favors higher spin states and another functional such as BPW91 with 6-311+G* basis set predicts that the singlet FeO_3 ($^1A_1'$) is below the quintet $FeOO_2$ ($^5B_2$) by 1.38 eV, $FeOO_2$ is not considered to be significantly populated in the experiments.

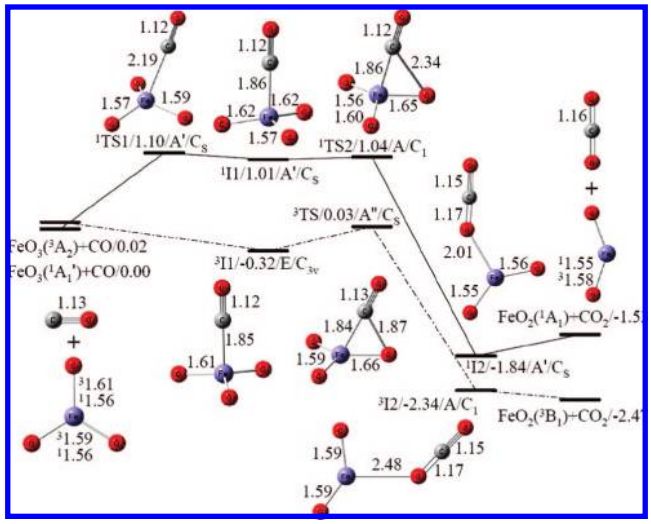

Figure 5. DFT calculated reaction pathways for FeO_3 ($^1A_1'$) + CO ($^1\Sigma^+$) → FeO_2 ($^1A_1$) + CO_2 ($^1\Sigma_g^+$) and FeO_3 ($^3A_2$) + CO ($^1\Sigma^+$) → FeO_2 ($^3B_1$) + CO_2 ($^1\Sigma_g^+$). See the caption of Figure 3 for explanations. All of the energies are relative to the total free energy of FeO_3 ($^1A_1'$) and CO ($^1\Sigma^+$).

(ORB) of 0.24 eV is determined for the reaction of ground-state FeO with CO (Figure 3). In Figure 4, although the B3LYP/6-311+G* predicts that the quintet FeO_2 ($^5B_2$) is slightly lower in energy (by 0.12 eV) than the triplet FeO_2 ($^3B_1$), previous experimental and theoretical studies have shown that the FeO_2 has a triplet ground state.[25,28b] Therefore, the reaction between the CO and FeO_2 should proceed in the triplet spin state in the experiment. The results in Figure 4 show that no ORB (or negative ORB of −0.08 eV) exists for CO reacting with FeO_2 in the experimentally determined spin state. The negative ORB for the FeO_2 + CO system is consistent with its high reactivity [$\sigma(FeO_2 + CO) > (3.4 \pm 1.3) \times 10^{-17}$ cm^2].

The DFT calculation (Figure 5) predicts that the FeO_3 has a singlet ground state ($^1A_1'$, D_{3h} point group) and the triplet state ($^3A_2$, C_{2v}) is above the ground state by 0.020 eV (it is 0.054 eV[42] for the zero-point-vibration corrected energy). A high ORB of 1.10 eV is present for CO approaching singlet FeO_3, whereas the ORB is very low (0.03 eV) for CO approaching triplet FeO_3. As the theoretical calculations are not accurate to 0.05 eV, the true ground state of FeO_3 may well be the triplet state. In this case, the DFT result can be used to explain the observed reactivity [$\sigma(FeO_3 + CO) \sim 1 \times 10^{-17}$ cm^2].

In the case that the triplet state of FeO_3 is slightly higher in energy than the singlet (such as the relative energies predicted by the B3LYP/6-311+G* in this study), a spin inversion mechanism[43] may be considered to explain the observed reactivity of FeO_3 (Figure 1). Figure 6 shows the potential energy curves for CO approaching FeO_3. CO approaches FeO_3 in the singlet spin state up to the Fe−C distance of 0.2967 nm. The spin inversion of the species from singlet to triplet spin state can happen at this point. Because the system energy at this conversion point is only 0.06 eV higher than that of the separated reactants (singlet FeO_3 + CO), formation of the triplet FeO_3CO species (^{3}I1 in Figure 5) is not subject to a significant energy barrier. This explains the observed reactivity of FeO_3 toward CO, as depicted in Figure 5. On the other hand, the spin inversion and the small barrier (0.06 eV) will be rate-limiting factors for singlet FeO_3 reacting with CO at $T \sim 350$ K. As a result, the observed reactivity of FeO_3 is lower than that of FeO_2, as experimentally observed.

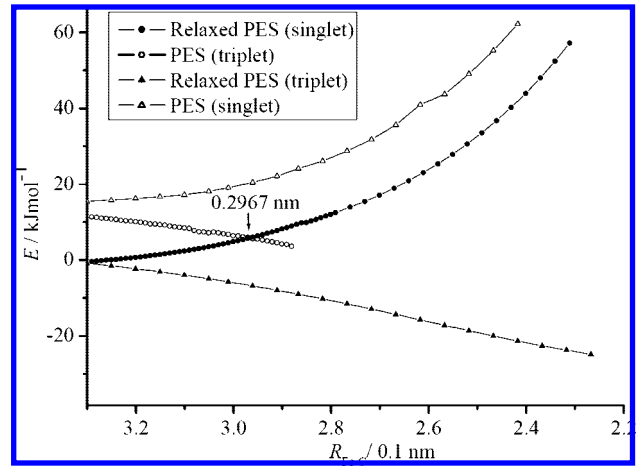

Figure 6. DFT calculated potential energy surfaces (PESs) for the FeO_3CO species by varying the Fe−C distance (R_{Fe-C}). The energy (E) is relative to the total electronic energy of FeO_3 ($^1A_1'$) and CO ($^1\Sigma^+$). The solid circles (●) and solid triangles (▲) denote the *relaxed* PESs of the singlet and triplet states of FeO_3CO, respectively. The *relaxed* PESs are obtained by partial geometry optimizations of FeO_3CO with Fe−C distance being fixed at various values. The PES denoted by the hollow circles (○) is calculated for triplet FeO_3CO by using the partially optimized geometries of the singlet FeO_3CO. The PES denoted by the hollow triangles (△) is calculated for the singlet FeO_3CO by using the partially optimized geometries of the triplet FeO_3CO.

The structures of neutral Fe_2O_{3-5} clusters are not well studied. Figures S1−S3 (see the Supporting Information) plot the lowest energy structures of Fe_2O_{3-5} with different conformers and spin multiplicities. The ground state of Fe_2O_3 is composed of a four membered ring (−Fe−O−Fe−O−) and a terminal Fe−O bond; Fe_2O_4 has a similar structure with an additional terminal Fe−O bond. The ground state of Fe_2O_5 (^{9}C1) is found to contain a peroxy unit with an O−O bond length of 0.132 nm. The structures with three (^{7}C2) or four (^{7}C3) Fe−O terminal bonds are higher in energy by ~0.5 eV. Because a high barrier (>1 eV, see Figure S4 in the Supporting Information) separates conformer C1 from conformers C2 and C3, Fe_2O_5 clusters with C1, C2, and C3 structures may be formed in our laser-ablation/supersonic-expansion conditions.

The reaction pathway shown in Figure 7 predicts that the oxidation of CO by the ground and low-lying excited states of Fe_2O_4 is subject to significant ORBs (0.23 and 0.35 eV). The reaction of Fe_2O_5 with CO is complicated due to possible existence of several conformers (C1−C3 in Supporting Information Figure S3). A tedious DFT investigation confirms that the reactions are all subject to significant ORBs (see Supporting Information Figure S5, parts A and B, for examples of reaction pathways): ORB (relative to the separated CO and the individual conformer) = 0.21 eV (^{7}C1), 0.39 eV (^{9}C1), 0.38 eV (^{11}C1), 0.26 eV (^{5}C2), 0.34 eV (^{7}C2), 0.46 eV (^{5}C3), and 0.68 eV (^{7}C3). In the reaction of CO with the C2 conformer of Fe_2O_5, CO may be oxidized by one of the two Fe−O terminal bonds on the same iron atom (Fe−O bonds on the right side, C2 in Figure S3 in the Supporting Information). In this case, the ORBs of 1.02 and 1.11 eV are determined for Fe_2O_5(^{5}C2) + CO and Fe_2O_5(^{7}C2) + CO, respectively.

The positive ORBs of the $Fe_2O_{4,5}$ + CO systems are consistent with the nonreactivity of $Fe_2O_{4,5}$ presented in Figure 1. Good agreement between the DFT calculations and the experimental observations has been achieved in this study. This

(43) Schröder, D.; Shaik, S.; Schwarz, H. *Acc. Chem. Res.* **2000**, *33*, 139.

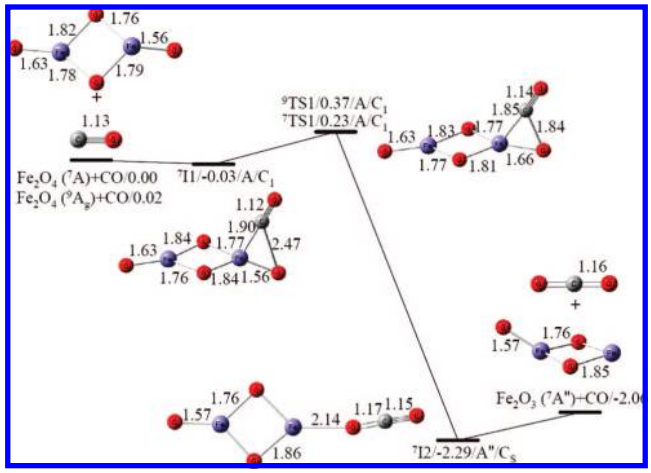

Figure 7. DFT calculated reaction pathway for Fe_2O_4 (^7A) + CO ($^1\Sigma^+$) → Fe_2O_3 ($^7A''$) + CO_2 ($^1\Sigma_g^+$). See the caption of Figure 3 for explanations. The transition state (TS1) is also optimized for spin multiplicity of 9. All of the energies are relative to the total free energy of Fe_2O_4 (^7A) and CO ($^1\Sigma^+$).

agreement between theory and experiment enables us to draw qualitative conclusions concerning the mechanisms of CO oxidation on Fe_mO_n clusters based on the DFT results.

4. Discussion

4.1. Mechanisms of CO Oxidation by Iron Oxide Clusters in the Gas Phase. Figures 3−5, 7, and Supporting Information Figure S5 show very similar processes of CO oxidation on different iron oxide clusters, even though the relative energies of the reaction intermediates and transition states depend on the individual clusters and their spin states. The first step in these reactions involves CO adsorption onto the clusters by carbon−iron interaction to form species $O_nFe_{m-1}Fe-CO$. The oxygen−iron interactions ($O_nFe_{m-1}Fe-OC$) are also explored. The species formed in this way are usually unstable or very high in energy. Direct CO_2 formation (carbon−oxygen interaction, such as $O_{n-1}Fe_mO-CO$) is also tested, as well. The reaction barriers are much higher than those presented in Figures 3−5, 7, and Supporting Information Figure S5. For the oxidation of CO by anionic AuO_n^- clusters, the initial complex formation involves a carbon−oxygen interaction: the CO molecule is able to bind directly to the oxygen atom in AuO_n^-.[9f] This could be an intrinsic mechanism difference between the CO oxidation over noble metal and over non-noble metal catalysts. A natural bond orbital (NBO) analysis[44] is performed to check the character of the carbon−iron interaction in the initial intermediates. The results are given in Table S2 in the Supporting Information. The interaction mainly involves electron donation from the lone pair orbital of the carbon atom to 4s and 3d orbitals of the iron atom. The involved carbon atomic orbitals are 2s (contribution >60%), $2p_x$, and $2p_y$. The iron 4s, $3d_{x^2-y^2}$, $3d_{z^2}$, and $3d_{xy}$ orbitals are generally involved in the interaction. Note that for reaction of Fe_2O_5 (^{7}C1) + CO (Figures S3 and S5A in the Supporting Information), iron $3d_{xz}$ and $3d_{yz}$ are involved in the interaction for species ^{7}I1.

After the initial intermediate formation through carbon−iron interactions, the second critical step of the reaction involves one terminal Fe−O bond activation. This is clearly demonstrated in Figures 3−5, 7, and Supporting Information Figure S5, in which the activated Fe−O bond lengths (in 0.1 nm in the list below) of the first transition states are significantly longer than those of the initial intermediates: 1.74 versus 1.62 for FeO ($^5\Delta$) + CO; 1.67 versus 1.59 for FeO_2 ($^3B_1$) + CO; 1.66 versus 1.61 for FeO_3 ($^3A_2$) + CO; 1.66 versus 1.56 for Fe_2O_4 (^7A) + CO; 1.71 versus 1.64 (Supporting Information Figure S5A) or 1.63 (Supporting Information Figure S5B) for Fe_2O_5 (^7A or $^7A''$) + CO. The activation energy ranges from 0.84 (FeO/$^5\Delta$ + CO) to 0.26 eV (Fe_2O_4/^7A + CO) with respect to the initial intermediates. Following Fe−O bond activation, the reaction is driven by additional C═O bond formation which is facile due to favorable thermodynamics: CO_2 (O−CO) bond enthalpy at 298 K is 5.54 eV, whereas those of FeO_{1-3} and Fe_2O_{4-5} are 4.29 (FeO/$^5\Delta$ → Fe/^{5}D + O/^{3}P), 3.59 (FeO_2/$^3B_1$ → FeO/$^5\Delta$ + O/^{3}P), 3.05 (FeO_3/$^1A_1'$ → $^3FeO_2$/$^3B_1$ + O/^{3}P), 3.25 (Fe_2O_4/^{7}C1/A → Fe_2O_3/^{9}C1/B_2 + O/^{3}P), and 2.93 (Fe_2O_5/^{7}C1/A → Fe_2O_4/^{7}C1/A + O/^{3}P) eV, based on our calculations. The experimental bond enthalpies of NO_2 (O−NO) and SO_3 ($O-SO_2$) at 298 K are 3.15 and 3.61 eV,[40] respectively. These two values are larger than the calculated bond enthalpies of FeO_3 and Fe_2O_5; thus, oxidation of NO and SO_2 by FeO_3 and Fe_2O_5 is thermodynamically favorable. The observed reactivity of FeO_3 and Fe_2O_5 toward NO and SO_2 (Figure 2) may be related to the oxidation reactions.

On the basis of experimental observations,[45] a two-state reactivity (TSR) that involves conversion of the reaction complex from one spin state to another was proposed as a new concept in organometallic chemistry.[43] The TSR has been recognized to be important in many reaction systems involving transition metals.[46] The spin conversion is predicted to occur in the late stage of the FeO_2 + CO reaction (Figure 4). A spin inversion point at which triplet $FeOCO_2$ can convert to quintet $FeOCO_2$ is shown in Figure S6 in the Supporting Information. The LIF technique could be employed to monitor the relative abundance of FeO products in different spin states. Because the spin conversion shown in Supporting Information Figure S6 occurs "after the transition state" (the critical barrier has been overcome along the IRC), such a spin conversion would have no effect on the rate measured in the present work.

Spin conversion may be considered (Figure 6) for the reaction of FeO_3 with CO in the case that the true ground state of FeO_3 is the singlet; however, no solid experimental evidence for such an occurrence exists and current theoretical calculations are not accurate enough to address this issue. The reactions of CO with FeO_3 in the singlet ($^1A_1'$) and in the triplet ($^3A_2$) states are subject to very high (1.10 eV) and very low (0.01 eV) ORBs (Figure 5), respectively. The observed reactivity of FeO_3 with CO (note that all of the FeO_3 clusters are reacted away if a high density of CO molecules is used in the experiment, not

(44) (a) Foster, J. P.; Weinhold, F. *J. Am. Chem. Soc.* **1980**, *102*, 7211. (b) Reed, A. E.; Curtiss, L. A.; Weinhold, F. *Chem. Rev.* **1988**, *88*, 899.

(45) (a) Hanton, S. D.; Noll, R. J.; Weisshaar, J. C. *J. Phys. Chem.* **1990**, *94*, 5655. (b) Fisher, E. R.; Armentrout, P. B. *J. Am. Chem. Soc.* **1992**, *114*, 2039. (c) Fisher, E. R.; Armentrout, P. B. *J. Am. Chem. Soc.* **1992**, *114*, 2050. (d) Schröder, D.; Schwarz, H.; Clemmer, D. E.; Chen, Y.; Armentrout, P. B.; Baranov, V. I.; Böhme, D. K. *Int. J. Mass Spectrom. Ion Processes* **1997**, *161*, 175.

(46) (a) Ogliaro, F.; Harris, N.; Cohen, S.; Filatov, M.; de Visser, S. P.; Shaik, S. *J. Am. Chem. Soc.* **2000**, *122*, 8977. (b) Shiota, Y.; Yoshizawa, K. *J. Am. Chem. Soc.* **2000**, *122*, 12317. (c) de Visser, S. P.; Ogliaro, F.; Harris, N.; Shaik, S. *J. Am. Chem. Soc.* **2001**, *123*, 3037. (d) Schoneboom, J. C.; Cohen, S.; Lin, H.; Shaik, S.; Thiel, W. *J. Am. Chem. Soc.* **2004**, *126*, 4017. (e) Hirao, H.; Kumar, D.; Que, L.; Shaik, S. *J. Am. Chem. Soc.* **2006**, *128*, 8590. (f) Michelini, M. C.; Russo, N.; Sicilia, E. *J. Am. Chem. Soc.* **2007**, *129*, 4229.

(47) Beyer, T.; Swinehart, D. R. *Commun. ACM* **1973**, *16*, 379.

shown in Figure 1) thus implies one of the two following options: (1) the triplet state is the ground state of FeO_3, or (2) the triplet state is the low-lying excited state of FeO_3. Figure 6 shows that the triplet state cannot be very high in energy above the singlet state, otherwise the energy of the spin conversion point will be too high for the reaction to occur, which is in disagreement with the observed reactivity of FeO_3 toward CO. To reach a definite conclusion on the TSR issue for reaction of FeO_3 with CO, further experimental and theoretical studies are required to determine the accurate energetics of the ground and low-lying excited states of FeO_3.

Figure 1 indicates that no association products (Fe_mO_nCO) or reaction intermediates such as I1 in Figures 3−5, 7, and Supporting Information Figure S5, are observed. The collision rate between the clusters and the helium bath gas molecules is about 10^8 s^{-1} under the employed experimental conditions. As a result, the lifetime (τ) of the reaction intermediates must be longer than 10 ns in order that they can be efficiently collision-stabilized in the fast flow reactor and detected in the TOFMS chamber. The initially formed (metastable) reaction intermediates, Fe_mO_nCO (I1 in Figures 3−5, 7, and Supporting Information Figure S5), carry vibrational energies (E_{vib}) of Fe_mO_n and CO at T_{vib} = 300−400 K, the binding energy (E_b) between Fe_mO_n and CO, and the center of mass kinetic energy ($E_k = \mu v^2/2$, μ—reduced mass of CO with Fe_mO_n, v = 800−1200 m/s). The Rice−Ramsberger−Kassel−Marcus (RRKM) theory can be used for computations of the rate constants of internal conversion (I1 → TS1 → I2 in Figures 3−5, 7, and Supporting Information Figure S5) or direct dissociation (Fe_mO_nCO/I1 → Fe_mO_n + CO):

$$k(E) = gN^{\ddagger}(E - E^{\ddagger})/\rho(E)/h \qquad (2)$$

in which g is the symmetry factor ($g = n$ for internal conversion of FeO_nCO, and $g = 1$ for internal conversion of $Fe_2O_{4,5}CO$ and all of the direct dissociations), $\rho(E)$ denotes the density of states of the metastable intermediates at the energy E [= $E_{vib}(Fe_mO_n) + E_{vib}(CO) + E_b + E_k$], $N^{\ddagger}(E - E^{\ddagger})$ represents the total number of states of the transition state (activated complex) with a barrier $E^{\ddagger}$ (E_b and $E^{\ddagger}$ are zero-point-vibration corrected energies), and h is the Planck constant. The direct count method proposed by Beyer and Swinehart[47] is used for determining the number ($N^{\ddagger}$) and density (ρ) of states under the approximation of harmonic vibrations. The E_{vib}, E_b, $E^{\ddagger}$, and vibrational frequencies are all from the DFT calculations. For the case that no distinct transition state exists on the potential energy surface (direct dissociation), one can consider different positions for the transition state along the reaction path and calculate rate constants corresponding to each of them. The minimum rate so obtained is the closest to the truth, assuming that quantum effects related to tunneling and nonseparability are negligible. This procedure is called the variational transition state theory (VTST).[38b] VTST calculations involve partial geometry optimizations (plus frequency calculations) by fixing Fe−C distances for the Fe_mO_nCO complex at various values. This procedure has only been performed for $^3FeO_{2,3}CO \rightarrow {}^3FeO_{2,3} + CO$ and $^7Fe_2O_4CO \rightarrow {}^7Fe_2O_4 + CO$.

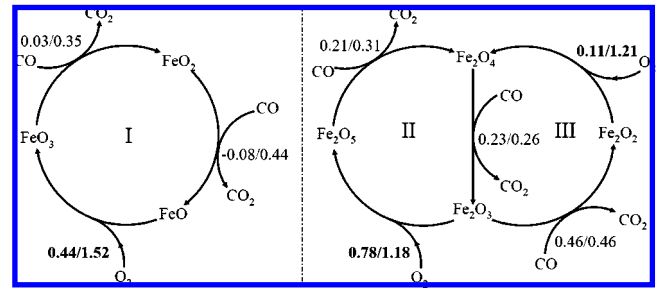

Figure 8. Three model catalytic cycles for the CO oxidation by O_2 over FeO_{1-3} and Fe_2O_{2-5}. The overall reaction barrier (ΔG_{ORB}) and the corresponding absolute reaction barrier (ΔG_{ARB}) in eV for each elementary step are given as $\Delta G_{ORB}/\Delta G_{ARB}$.

Supporting Information Table S3 lists the rate constants computed with eq 2. All of the internal conversions ($FeO_{1-3}CO$ and $Fe_2O_{4-5}CO$: I1 → TS1 → I2) have rate constants greater than 4×10^9 s^{-1}. This means that the lifetimes of the metastable reaction intermediates (I1 in Figures 3−5, 7, and Supporting Information Figure S5) are too short (τ < 0.25 ns) for the reaction intermediates Fe_mO_nCO to be observed in the experiment. The RRKM computations predict that the direct dissociation of Fe_2O_4CO ($^7I1 \rightarrow Fe_2O_4 + CO$) is significantly faster than the internal conversion ($^7I1 \rightarrow {}^7TS1 \rightarrow {}^7I2$). Similar behavior is expected for Fe_2O_5CO as can be seen from the similarity between the reaction paths in Figure 7 and Supporting Information Figure S5. In contrast, the rate constants of the direct dissociations of $FeO_{2,3}CO$ are smaller than those of internal conversions under conditions T_{vib} = 350 K and v = 1000 m/s. These are qualitatively in agreement with the experimental results in Figure 1: $FeO_{2,3}$ are reactive, whereas $Fe_2O_{4,5}$ are not reactive in reactions with CO.

4.2. Catalytic Cycles in the Gas Phase. In the practical catalytic oxidation of CO by O_2, the catalysts (iron oxides) have to be cycled. Figure 8 presents three model catalytic cycles (I−III) by using FeO_{1-3}, Fe_2O_{3-5}, and Fe_2O_{2-4} as catalysts for CO oxidation. The reaction pathways for $Fe_2O_3 + O_2 \rightarrow Fe_2O_5$, $FeO + O_2 \rightarrow FeO_3$, $Fe_2O_3 + CO \rightarrow Fe_2O_2 + CO_2$, and $Fe_2O_2 + O_2 \rightarrow Fe_2O_4$ are given in Supporting Information Figures S4, S7, S8, and S9, respectively. Each of the O−O bond breaking processes is subject to a high [$FeO + O_2$, 1.52 eV ($^5TS2 - {}^5I2$, Supporting Information Figure S7); $Fe_2O_2 + O_2$, 1.21 eV ($^{11}TS2 - {}^{11}I2$, Supporting Information Figure S9A); $Fe_2O_3 + O_2$, 1.18 eV ($^9TS2 - {}^9I2$, Supporting Information Figure S4)] absolute reaction barrier (ARB), defined as the energy difference between the transition state (TS) and the intermediate through which the TS is generated. The rate-limiting steps of cycles I and II are the O−O bond activation (or breaking) processes that are subject to both high ORBs and ARBs.

(48) The experimental work (Figure 1) suggests that single-iron sites ($FeO_{2,3}$ as models) are active, whereas two-iron assemblies ($Fe_2O_{4,5}$ as models) are not, for the oxidation of CO; however, in the model catalytic cycles (FeO_{1-3} and Fe_2O_{3-5} as model catalysts, see cycles I and II in Figure 8), the most difficult (rate-limiting) step is O−O bond breaking. We thus give up choosing single irons as the best catalytic sites when plotting Figure 9. Although $Fe_2O_{4,5}$ clusters do not oxidize CO under the employed gas-phase conditions (limited CO pressure, bath gas cooling rate, and reaction time), two-iron assemblies on the surface of catalysts can coordinate a CO molecule as long as the rate constant for energy dissipation through surface phonons and bath gases is fast enough ($\geq 10^{11}$ s^{-1}, see the rate of direct dissociation of $Fe_2O_4/{}^7I1 \rightarrow Fe_2O_4 + CO$ in Table S3 in the Supporting Information). After the coordination, the oxidation of CO by the catalyst is subject to low (≤0.31 eV in cycle II of Figure 8) ARBs. In the study of O−O bond breaking over Fe_2O_3 (Supporting Information Figure S4), $(FeO)_{1,2}$ (Supporting Information Figures S7 and S9), and Fe_2O (Supporting Information Figure S10), the ARBs are high (>1 eV) if the average oxidation state of iron (AOS) in the clusters is greater than or equal to +2 [in Fe_2O_3 and $(FeO)_{1,2}$], whereas the ARBs can be low (≤0.54 eV) if the AOS of iron is +1 (in Fe_2O). We thus put an iron (instead of an oxygen) atom in site C when plotting Figure 9. It should be mentioned that the mechanisms of a practical heterogeneous catalysis are very complex. Figure 9 represents one possible idea for how CO oxidation by O_2 may be efficiently catalyzed by the iron oxides.

The rate-limiting step of cycle III is not apparent because the O−O ($Fe_2O_2 + O_2 \rightarrow Fe_2O_4$) activation has a smaller ORB and a much higher ARB than the Fe−O activation (such as $Fe_2O_3 + CO \rightarrow Fe_2O_2 + CO_2$) does. In the absence of bath gas cooling, RRKM theory (eq 2) can be used to calculate the rate constant for O−O bond breaking (I2 → TS2 → I3, Supporting Information Figure S9A). The computed rate constant is between 1.96×10^7 and 5.78×10^7 s^{-1} (see the last line of Table S3 in the Supporting Information). The rate constant of bath gas collision is about 10^8 s^{-1} under conditions of $P = 14$ Torr and $T = 350$ K. This means that the binding energy (1.10 eV) is likely to be dissipated into the bath through collisions under high-pressure conditions ($P > 14$ Torr). After energy dissipation, the O−O activation (cycle III) will be subject to a very high barrier (1.21 eV) compared to the Fe−O activations (0.23−0.46 eV). We may conclude that the O−O activation is also the rate-limiting step in cycle III under the conditions of high bath gas pressure (>14 Torr). Note that gas pressure of 10−100 Torr ($CO + O_2$) is usually used in the condensed phase catalytic studies.[18]

4.3. Understanding of the Condensed Phase Catalytic Oxidation of CO at a Molecular Level. The redox mechanism, by which (I) CO is oxidized by the oxygen of the catalyst and (II) the reduced catalyst is oxidized by gas-phase O_2, is suggested for CO oxidation over iron oxide catalysts.[15b,16] On the basis of this general mechanism, the findings for the investigation of CO oxidation catalyzed by small neutral iron oxide clusters in this study can be used to rationalize interesting phenomena observed for the related condensed phase catalysis at a molecular level. Szegedi et al. found that iron oxide catalysts treated (oxidized) at 625 K with O_2 show very low reactivity, whereas the catalysts treated (reduced) above 773 K with H_2 show high reactivity.[18] The following paragraph discusses how this surface oxidation/reduction issue may be related to both aspects (I and II) of the redox mechanism at a molecular level.

Figures 3−5, 7, and Supporting Information Figure S5 indicate that an iron center has to be provided for the initial intermediate (Fe_mO_nCO/I1) formation through a carbon−iron interaction because the direct CO_2 formation through the carbon−oxygen interaction is subject to high reaction barriers. For an oxygen-saturated surface treated with O_2 at high temperature, the CO has less chance to approach iron. The CO has a weaker interaction with an oxygen-saturated iron center than with an oxygen-unsaturated iron center, which may lead to a higher Fe−O bond activation barrier for an oxygen-saturated iron center than for an oxygen-unsaturated iron center. This point is demonstrated by examining CO oxidation on Fe_2O_5 clusters with C2 structure (Supporting Information Figure S3). The Fe−O activation barriers are higher for the Fe−O bond on the iron atom connected to four O atoms, than for the one on the other iron atom connected to three O atoms (1.0−1.1 eV vs 0.2−0.3 eV). On the other hand, for a reduced surface treated with H_2 at high temperature, more iron centers are present for O_xFe-CO complex formation. This point is confirmed by the conclusion of ref 17d that the high density of Fe atoms on exposed {110} planes leads to high catalytic performance of the quasicubic α-Fe_2O_3 nanocrystals. Szegedi et al. also finds that treatment (dehydroxylation) in high-temperature He after H_2 reduction further improves the high reactivity of the catalyst.[18] This means that the existence of FeOOH species, interpreted to be important for the catalyst reactivity,[16] may not be required. This is again in agreement with the suggested mechanism that carbon−iron interaction is important to initiate the CO oxidation by catalyst.

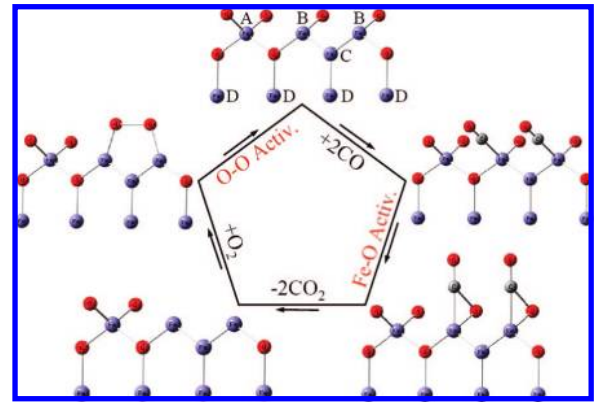

Figure 9. Possible catalytic cycle for the CO oxidation by O_2 over iron oxide catalysts at the molecular level. A, B, and C mark different surface Fe atoms while D marks lattice Fe atoms that are underneath the surface.

Szegedi et al. found that the efficient condensed phase iron-containing catalysts (treated with H_2/He at high temperature) have both ionic and metallic forms of iron. The metallic form of iron is suggested to play a role in *CO activation* through interaction of a metal ion, stabilized in the neighborhood of a supported metal nanocluster ("metal ion−metal nanocluster" ensemble site), with the lone pair of the oxygen atom of a chemisorbed CO molecule.[18] The study in this work shows no evidence of interaction between the oxygen atom of CO and a metal ion (Fe^{3+}, Fe^{2+}) in the Fe_mO_n clusters. The mechanism of CO_2 formation over Fe_mO_n is quite simple: interaction of a lone pair of carbon with an iron atom and subsequent activation of an Fe−O bond that causes formation of another C═O bond. The Fe−O activation barrier is either negative or quite low (0.03−0.46 eV). These imply that the *CO activation* process suggested in ref 18 may not be required.

Another important aspect of the redox mechanism is the O−O bond breaking (or O_2 activation) over the catalysts. In all of the three model catalytic cycles (Figure 8) proposed, the process of the O−O bond breaking is the rate-limiting step. This suggests that efficient O_2 activation should be considered in practical catalysis. In Supporting Information Figure S4, the process of O−O bond breaking over Fe_2O_3 is subject to high ORBs (≥0.78 eV) and high ARBs (≥1.18 eV). In sharp contrast (see Figure S10 in the Supporting Information), the ORBs are negative and the ARBs can be small (≤0.54 eV, Supporting Information Figure S10B) for the O−O bond breaking over Fe_2O, in which the iron atoms can be considered to be metallic. The metallic form of iron found in efficient iron-containing catalysts[18] is thus suggested to be important for O_2 activation (rather than the *CO activation*).

Our understanding of CO oxidation by O_2 catalyzed by iron oxides at a molecular level is displayed in Figure 9 (some notes are given in ref 48). Metallic (C), cationic (B), and overoxidized (A) surface Fe atoms (or sites) may be present in iron oxide catalysts prepared by different procedures. The overoxidized site A is not very catalytic because Fe is covered by too many O atoms that prevent CO/Fe coordination. The cationic site B is reactive toward CO oxidation by coordinating CO through carbon−iron interaction and subsequent Fe−O activation. The metallic site C promotes O−O activation over sites B or BCB,

and we suggest that a site like BCB is very catalytic for the CO oxidation by O_2.

5. Conclusions

Single-photon ionization and DFT calculations are successfully applied for investigation of the reactivity of small neutral iron oxide clusters toward CO. Cluster size-dependent reactivity is observed and well interpreted by the DFT calculations. Two essential steps are present in the oxidation of CO by Fe_mO_n clusters: (1) the initial intermediate formation that involves carbon−iron interaction and (2) the Fe−O bond activation that determines the overall reaction barrier. The Fe−O bond activation energy at room temperature varies from −0.08 (FeO_2) to 0.46 eV (Fe_2O_3). Three model catalytic cycles for CO oxidation by O_2 facilitated by FeO_{1-3}, Fe_2O_{3-5}, and Fe_2O_{2-4} clusters are studied by DFT calculations, and all of the rate-limiting steps involve the O−O activation. The findings in this gas-phase study can be used to rationalize interesting phenomenon in related condensed phase catalysis at a molecular level. In the process of CO oxidation by O_2, the oxygen overoxidized iron sites are not very catalytic, whereas the reduced cationic and metallic forms of iron, in efficient iron oxide catalysts, are suggested to be important for Fe−O and O−O activations, respectively.

Acknowledgment. This work was supported by Philip Morris, U.S.A., the U.S. DOE BES program, the NSF ERC for Extreme Ultraviolet Science and Technology under NSF Award No. 0310717, the National Center for Supercomputing Applications under Grant CHE070000N, the Chinese Academy of Sciences (Hundred Talents Fund), the National Science Foundation of China (No. 20703048), and the 973 Programs (Nos. 2006CB932100 and 2006CB806200).

Supporting Information Available: Complete ref 31, DFT/6-311+G* calculated and experimental bond lengths and bond enthalpies for O_2, CO, CO_2, FeO molecules (Table S1), structures of Fe_2O_{3-5} clusters (Figures S1−S3), reaction pathways for $Fe_2O_3 + O_2$ and $Fe_2O_5 + CO$ (Figures S4 and S5), carbon−iron interaction from the NBO analysis of the initial intermediates in the reactions of FeO_{1-3} and Fe_2O_{4-5} with CO (Table S2), potential energy curve crossing in $FeO_2 + CO$ (Figure S6), rate constants of internal conversion or direct dissociation of $FeO_{1-3}CO$, $Fe_2O_{4,5}CO$, and $Fe_2O_2O_2$ computed from the RRKM theory (Table S3), reaction pathways for $FeO + O_2$, $Fe_2O_3 + CO$, $Fe_2O_2 + O_2$, and $Fe_2O + O_2$ (Figures S7−S10), and Cartesian coordinates, electronic energies, and vibrational frequencies for all of the optimized structures (Tables S4−S14). This material is available free of charge via the Internet at http://pubs.acs.org.

JA8023093